Parathyroid hormone(1–34) and its analogs differentially modulate osteoblastic *Rankl* expression via PKA/SIK2/SIK3 and PP1/PP2A–CRTC3 signaling

Received for publication, July 5, 2018, and in revised form, October 17, 2018 Published, Papers in Press, October 30, 2018, DOI 10.1074/jbc.RA118.004751

Florante R. Ricarte[‡], Carole Le Henaff[§], Victoria G. Kolupaeva[§], Thomas J. Gardella[¶], and Nicola C. Partridge[‡§1]

From the [‡]Department of Biochemistry and Molecular Pharmacology, New York University School of Medicine, New York, New York 10016, the [§]Department of Basic Science and Craniofacial Biology, New York University College of Dentistry, New York, New York 10010, and the [¶]Endocrine Unit, Massachusetts General Hospital, Harvard Medical School, Boston, Massachusetts 02114

Edited by Henrik G. Dohlman

Osteoporosis can result from the loss of sex hormones and/or aging. Abaloparatide (ABL), an analog of parathyroid hormone–related protein (PTHrP(1–36)), is the second osteoanabolic therapy approved by the United States Food and Drug Administration after teriparatide (PTH(1–34)). All three peptides bind PTH/PTHrP receptor type 1 (PTHR1), but the effects of PTHrP(1–36) or ABL in the osteoblast remain unclear. We show that, in primary calvarial osteoblasts, PTH(1–34) promotes a more robust cAMP response than PTHrP(1–36) and ABL and causes a greater activation of protein kinase A (PKA) and cAMP response element–binding protein (CREB). All three peptides similarly inhibited sclerostin (*Sost*). Interestingly, the three peptides differentially modulated two other PKA target genes, *c-Fos* and receptor activator of NF-κB ligand (*Rankl*), and the latter both *in vitro* and *in vivo*. Knockdown of salt-inducible kinases (SIKs) 2 and 3 and CREB-regulated transcription coactivator 3 (CRTC3), indicated that all three are part of the pathway that regulates osteoblastic *Rankl* expression. We also show that the peptides differentially regulate the nuclear localization of CRTC2 and CRTC3, and that this correlates with PKA activation. Moreover, inhibition of protein phosphatases 1 and 2A (PP1/PP2A) activity revealed that they play a major role in both PTH-induced *Rankl* expression and the effects of PTH(1–34) on CRTC3 localization. In summary, in the osteoblast, the effects of PTH(1–34), PTHrP(1–36), and ABL on *Rankl* are mediated by differential stimulation of cAMP/PKA signaling and by their downstream effects on SIK2 and -3, PP1/PP2A, and CRTC3.

Osteoporosis is a prevalent disease in our aging population. Annually, more than 8.9 million osteoporotic fractures are reported worldwide, with a total cost of $25 billion (1). Standard treatment with bisphosphonates curtails bone resorption, but does not aid in forming new bone. Teriparatide, or PTH(1–34), was the first FDA-approved osteoanabolic therapy (2, 3) and studies aimed at delineating its effects on the skeleton remain under close investigation (4–6). The second and only other FDA-approved osteoanabolic treatment, abaloparatide (ABL),[2] is an analog of parathyroid hormone–related protein (PTHrP(1–34)), and phase III clinical trials reported that ABL was similar, if not superior, to teriparatide in increasing bone mineral density in osteoporotic, postmenopausal women (7). Interestingly, it was also reported that serum CTX levels, the marker for bone resorption, were significantly lower than in patients treated with teriparatide. Additionally, bone resorption markers were unperturbed in ovariectomized rats (8) and monkeys (9) treated with ABL compared with the ovariectomized control groups.

PTH(1–34), PTHrP(1–36), and ABL bind the same G protein–coupled receptor, parathyroid hormone receptor, type 1 (PTHR1), which is expressed in the cells of the osteoblast lineage, chondrocytes, and kidneys (10). Although a variety of signaling cascades are activated upon ligand-receptor binding (reviewed in Ref. 11), the $G\alpha_s$/cAMP pathway is known to mediate the bone anabolic response of PTH (12). Studies have described PTH signaling in the osteoblast/osteocyte (reviewed in Ref. 13) and its effects on their respective transcriptomes (14, 15), but the specific effects of PTH on the regulation of the pro-osteoclastogenic cytokine, receptor activator of NF-κB ligand (RANKL), are of great interest due to its central role in the cross-talk between osteoblasts/osteocytes and the bone resorbing cells of the skeleton, the osteoclast (16–22).

Recently, a study showed that in the osteocyte, PTH regulates *Rankl* expression through the inhibition of salt-inducible kinases (SIKs) and nuclear translocation of cAMP-regulated transcriptional coactivator, CRTC2 (23), which is a known substrate of SIKs (24). This study also reported that PTH-induced SIK inhibition allows for nuclear translocation of histone

This work was supported by National Institutes of Health Grants DK47420, DK47420S1, and T32 GM066704. The authors declare that they have no conflicts of interest with the contents of this article. The content is solely the responsibility of the authors and does not necessarily represent the official views of the National Institutes of Health.
This article contains Figs. S1–S3 and Tables S1 and S2.

[1] To whom correspondence should be addressed: Dept. of Basic Science and Craniofacial Biology, New York University College of Dentistry, 345 East 24th St., 902A, New York, NY 10010. Tel.: 212-992-7145; Fax: 212-992-4204; E-mail: ncp234@nyu.edu.

[2] The abbreviations used are: ABL, abaloparatide; PTHrP, parathyroid hormone–related protein; RANKL, receptor activator of NF-κB ligand; SIK, salt-inducible kinase; HDAC, histone deacetylase; PP2A, protein phosphatase 2A; PKA, protein kinase A; CREB, cAMP response element–binding protein; SOST, sclerostin; MMP, matrix metalloprotease; qRT, quantitative RT; myr-PKI, myristoylated PKA inhibitor; OA, okadaic acid; IBMX, isobutylmethylxanthine; FBS, fetal bovine serum; HRP, horseradish peroxidase; GFP, green fluorescent protein; DAPI, 4′,6-diamidino-2-phenylindole.

deacetylases, HDACs 4 and 5, which inhibit the transcription factor, MEF2c, and therefore decrease *Sost* expression (23). Previous studies have also reported differences in downstream PTHR1 effects between PTH(1–34), PTHrP(1–36), and ABL (25). Based on this, we hypothesized that in the osteoblast, PTH(1–34), PTHrP(1–36), and ABL would differentially modulate this particular signaling axis and ultimately result in differing effects on the regulation of *Rankl* mRNA. Additionally, because this cascade was reported to involve an unknown serine/threonine phosphatase and PTHrP is able to activate protein phosphatase 2A (PP2A) in the chondrocyte (26), we hypothesized that this activation would also be important in the osteoblast.

Here, we report that PTH(1–34), PTHrP(1–36), and ABL differentially induce cAMP/PKA signaling. Accordingly, different levels of PKA activation lead to differences in the up-regulation of *Rankl* mRNA by all three peptides, and we found that this phenomenon is a direct result of PKA activation. We also found that osteoblastic *Rankl* expression requires SIKs 2 and 3, CRTC3, and PP1/PP2A and that the three peptides, through PP1/PP2A, differentially regulate the nuclear translocation of CRTCs 2 and 3. Interestingly, PTH(1–34), PTHrP(1–36), and ABL equally inhibit osteoblastic *Sost* expression, which illustrates a demarcation between SIK/HDAC/MEF2c and SIK/CRTC signaling. Taken together, our data show that these peptides differentially regulate a particular arm of the cAMP/PKA/SIK signaling axis and ultimately result in lower expression of *Rankl* by ABL, which may provide an explanation for the decreased resorptive effects of ABL observed *in vivo*.

Results

PTH(1–34), PTHrP(1–36), and ABL similarly bind PTHR1

Previous studies aimed at comparing the binding efficacies between PTH(1–34) or PTHrP(1–36) with their cognate receptor, PTHR1, have shown that although both are able to bind with similar affinity, PTH(1–34) binds PTHR1 in both high affinity receptor conformations, R^0 (G-protein uncoupled) and R^G (G protein– coupled), whereas PTHrP(1–36) favors the latter (27). These differences were also reflected in the ability of PTH(1–34) to elicit a more sustained cAMP response upon receptor internalization, whereas PTHrP(1–36) could not (28). More recently, comparative studies between PTH(1–34), PTHrP(1–36), and ABL in GP-2.3 cells have shown that ABL binds more selectively to the R^G conformation of PTHR1, thus resulting in a more transient cAMP response compared with PTH(1–34) (25). To determine whether these differences were observable in osteoblastic cells, we measured the capacities of PTH(1–34), PTHrP(1–36), and ABL to compete for binding to PTHR1 in the osteosarcoma cell line, UMR 106, using [^{125}I-Nle^{8,21},Tyr^{34}]rPTH(1–34) as a tracer radioligand (Table 1). We found no significant difference in pIC_{50} between the three peptides under these conditions.

Table 1
Competition binding to the PTHR1 in UMR 106 cells

Peptide concentrations (as -Log M with corresponding nM value in parentheses), that inhibited by 50% the binding of [^{125}I-Nle^{8,21},Tyr^{34}]rPTH(1–34) to the PTHR1 in UMR 106 cells. Data are mean ± S.E. of four experiments with six (n = 2) or 3 (n = 3) replicate wells in each.

	pIC_{50}	p value
	*n*M	
PTH(1–34)	7.89 ± 0.10 (13.0)	1.00
PTHrP(1–36)	8.08 ± 0.12 (8.33)	0.270
ABL	7.57 ± 0.14 (26.8)	0.120
[Nle^{8,21},Tyr^{34}]rPTH(1–34)	8.56 ± 0.22 (2.73)	0.047

PTH(1–34) elicits a stronger cAMP response and downstream effects on PKA/CREB compared with PTHrP(1–36) and ABL

Because we did not observe differences in PTHR1 binding, we hypothesized that in primary murine calvarial osteoblasts, a system that more closely resembles the physiological setting, more pronounced differences that will integrate downstream signaling would be observed. Upon treating primary osteoblasts with PTH(1–34), PTHrP(1–36), or ABL, we found that all three peptides achieved maximal cAMP responses at 30 min, but PTH(1–34) resulted in higher cAMP concentrations (240 ± 23 pmol/μl), compared with PTHrP(1–36) (175 ± 4 pmol/μl) or ABL (45 ± 5 pmol/μl; Fig. 1*a*). Because cAMP levels are the rate-limiting step to PKA activation, we therefore sought to observe how these differing cAMP responses affected PKA activity. Indeed, we found that whereas all three peptides achieve peak PKA activation between 1 and 2 min, PTH(1–34) reached 72% PKA activation, whereas PTHrP(1–36) and ABL resulted in 50 and 30%, respectively (Fig. 1*b*). The differences in magnitude of each peptide's cAMP response were proportional to their effect on PKA activation. To assess the dose-dependent effects of these peptides, we performed a dose-response at 1 min and found that at 0.75 nM, PTH(1–34) resulted in 40% PKA activation, whereas PTHrP(1–36) and ABL elicited less than half of that at that dose (16 and 18%, respectively). Additionally, the relative differences in PKA activation between all three peptides grew smaller with larger doses, but ABL did not achieve the same levels of PKA activation (53%) as PTH(1–34) (73%) or PTHrP(1–36) (68%) (Fig. 1*c*). Previously, we reported that cAMP/PKA signaling leads to activation of the cAMP response element– binding protein (CREB) and the stimulation of c-*Fos* expression in osteoblastic cells (29, 30). We found that all three peptides resulted in maximal CREB activation (assayed by phosphorylation of CREB at Ser-133) at 5 min, and again, in proportions similar to their effects on cAMP/PKA (PTH(1–34) = 77%, PTHrP(1–36) = 55%, ABL = 20%; Fig. 1*d*). Dose-response of CREB activation at 5 min shows a similar curve as seen with PKA activation (Fig. 1*e*), thus confirming that the initial differences in cAMP response exerted by PTH(1–34), PTHrP(1–36), and ABL on cAMP are directly reflected in their downstream effectors, PKA and CREB.

PTH(1–34), PTHrP(1–36), and ABL differentially regulate osteoblastic genes c-Fos and Rankl

To determine the consequences, if any, of the initial signaling differences between PTH(1–34), PTHrP(1–36), and ABL on the regulation of osteoblastic genes, we performed time course and dose-response analyses, followed by qRT-PCR on a set of osteoblastic genes. After treating primary osteoblasts and/or osteoblastic UMR 106-01 cells with peptide concentrations ranging from 0.001 to 100 nM at 1, 2, and 4 h, we found no significant differences with almost all of the genes assayed (Table 2). PTH is a known regulator of sclerostin (*Sost*) (31) and

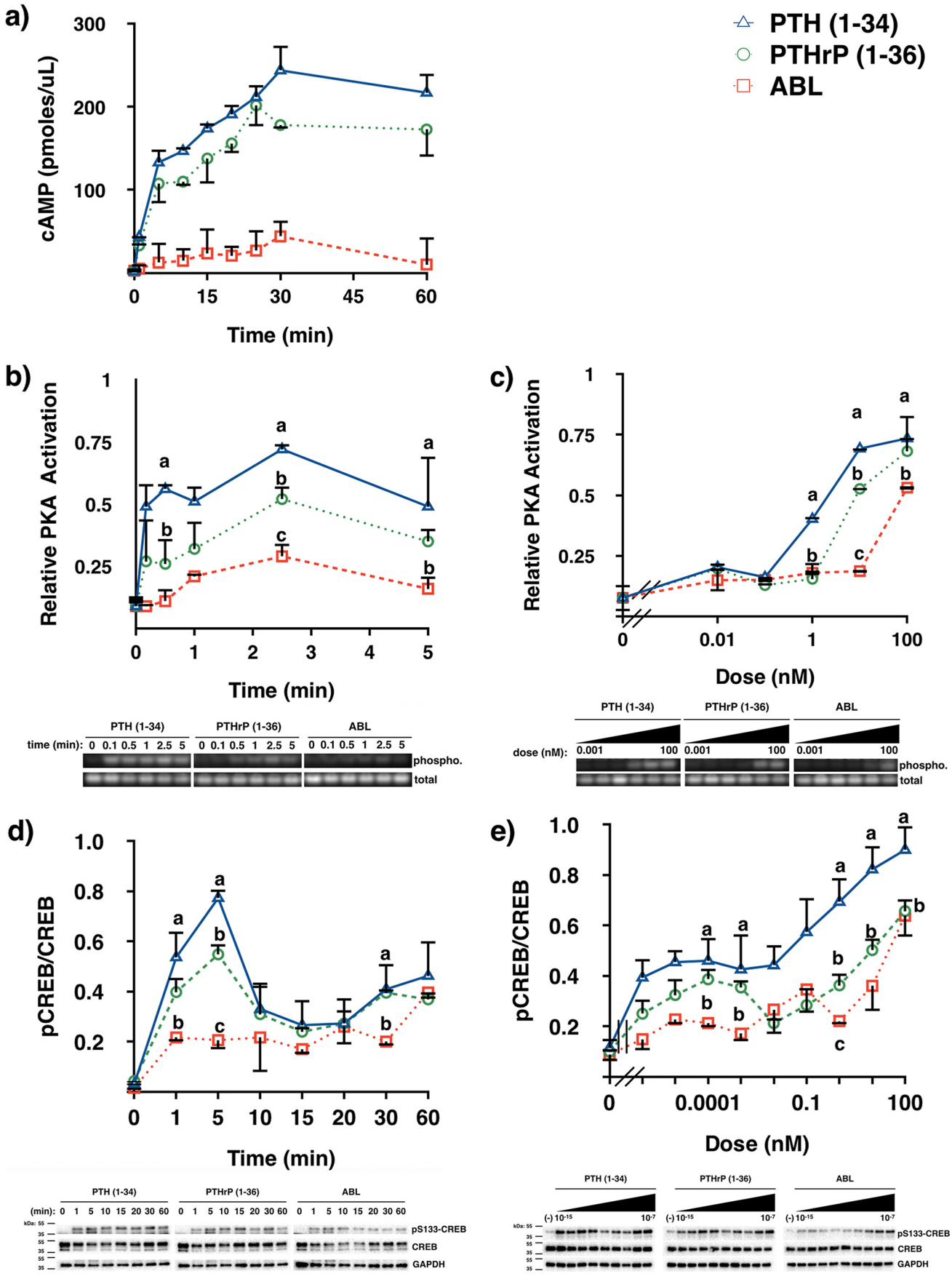
a)
cAMP (pmoles/uL)
Time (min)
PTH (1-34)
PTHrP (1-36)
ABL
b)
Relative PKA Activation
Time (min)
PTH (1-34)
PTHrP (1-36)
ABL
time (min):
phospho.
total
c)
Relative PKA Activation
Dose (nM)
PTH (1-34)
PTHrP (1-36)
ABL
dose (nM):
phospho.
total
d)
pCREB/CREB
Time (min)
PTH (1-34)
PTHrP (1-36)
ABL
(min):
pS133-CREB
CREB
GAPDH
e)
pCREB/CREB
Dose (nM)
PTH (1-34)
PTHrP (1-36)
ABL
pS133-CREB
CREB
GAPDH

Table 2

Comparative effects of PTH(1–34), PTHrP(1–36), and ABL on osteoblastic genes

Primary calvarial osteoblasts were treated with peptides for 1, 2, or 4 h with peptide doses ranging from 0.001 to 100 nM, followed by qRT-PCR. Messenger RNA abundance of each gene was analyzed relative to the housekeeping gene, *β-actin*, and represent the mean ± S.D. of $n = 3$ independent experiments.

Gene ID	Gene name	PTH	PTHrP	ABL
Ibsp	Bone Sialoprotein	–[a]	–	–
Sost	Sclerostin	–	–	–
Opg	Osteoprotegerin	NC	NC	NC
Alp	Alkaline phosphatase	+	+	+
Col1a1	Collagen, type 1	+	+	+
Runx2	Runt-related transcription factor 2	+	+	+
Mmp13	Matrix metalloproteinase 13	+	+	+
Mcp1	Monocyte chemoattractant protein-1	+	+	+
c-*Fos*	c-Fos	+++	++	+
Rankl	Receptor activator of nuclear factor κB ligand	+++	+	+

[a] –, decrease; +, increase; and NC, no change.

matrix metalloprotease (MMP) 13 (32) expression, and all three peptides led to a 2-fold increase in *Mmp13* mRNA in primary osteoblasts (Fig. 2*a*) and a complete suppression of *Sost* mRNA in UMR 106-01 cells (Fig. 2*b*), with no significant differences in the dose-response between the three peptides. Interestingly, both genes have been reported to be regulated by PTH in a cAMP/PKA/HDAC4/5-dependent mechanism (33, 34), suggesting that this arm of the cAMP/PKA signaling axis is similarly regulated by all three peptides, and likely is sensitive to low PKA activation. Because the inhibition of *Sost* represents one of the major anabolic effects of PTH, its identical inhibition by PTH(1–34), PTHrP(1–36), and ABL may account for the similar osteoanabolic effects observed *in vivo*.

Importantly, our analyses revealed two genes that were differentially regulated by the peptides: the transcription factor, c-*Fos*, and the pro-osteoclastogenic factor, *Rankl*. We have shown that c-*Fos* is an immediate-early downstream effector of PTH by way of cAMP/PKA signaling (29, 30), and here, we confirm peak c-*Fos* mRNA abundance at 1 h, where PTH(1–34) resulted in a 10-fold increase, whereas PTHrP(1–36) and ABL resulted in 5- and 4-fold increases, respectively, and all returned to basal levels by 4 h (Fig. 2*c*). Dose-response analysis of c-*Fos* mRNA abundance (Fig. 2*d*) mirrored the differential effects of all peptides on cAMP/PKA/CREB signaling and confirmed that in osteoblasts, PTHrP(1–36) and ABL are weaker effectors of this arm of cAMP/PKA signaling compared with PTH(1–34).

Rankl is a well-studied PTH-responsive gene in osteoblasts and osteocytes (16–18, 21, 35, 36) and here, we found peak fold-induction by all three peptides at 4 h and a significant difference in the effect of the peptides at 1 nM (PTH(1–34) = 8-fold, PTHrP(1–36) = 3-fold, ABL = 3-fold; Fig. 2, *e* and *f*). Due to the central role of RANKL as the driver of osteoclastogenesis and a mediator between osteoblasts/osteocytes and osteoclasts, we sought to investigate the differential effects of PTH(1–34), PTHrP(1–36), and ABL on osteoblastic *Rankl* expression.

Differential regulation of Rankl relies on the PKA/PP1/PP2A signaling axis in vitro

Rankl gene expression has been shown to be regulated by cAMP/PKA activity in vascular cells (37), mesenchymal stem cells (38), and osteocytes (21, 23), and due to the differential effects of PTH(1–34), PTHrP(1–36), and ABL on this signaling axis, we hypothesized that modulating PKA activity would abolish any differences they elicit in the osteoblast with respect to *Rankl* mRNA expression. Indeed, pre-treatment with the PKA agonist, 8-bromo-cAMP (8-Br-cAMP) alone increased *Rankl* mRNA levels by 38-fold and abolished the effects of all three peptides on RANKL, suggesting *Rankl* mRNA cannot be enhanced above a maximal level (Fig. 3*a*). Conversely, pre-treatment with the PKA-specific antagonist, myristoylated PKA inhibitor (myr-PKI), did not affect basal *Rankl* mRNA levels, but completely abolished the effects of all three peptides (Fig. 3*a*). To confirm these findings in a different system, we performed similar experiments with primary osteoblasts derived from bone chips of adult C57Bl/6 WT femurs and obtained identical results (Fig. S1).

Protein phosphatase 1 (PP1) and PP2A are two major Ser/Thr phosphatases that account for the majority of phosphatase activity in eukaryotes. PP1 activity is modulated through the formation of heterotrimeric complexes with numerous regulatory subunits. Targeting to specific substrates involves interaction of PP1 catalytic subunit C with targeting subunits, of which 30 have been identified (39). In skeletal muscle, PP1 activity has been shown to be indirectly regulated by PKA, because it directly phosphorylates a PP1 targeting subunit, G_M (40). PP2A has been implicated in the regulation of *Rankl* in MC3T3-E1 cells (41), in addition to its involvement in PTHrP signaling in the chondrocyte (26). PP2A holoenzymes consist of a dimer formed by a catalytic C subunit (PP2A-C) and scaffolding A subunit (PP2A-A), which is targeted to the substrate by a regulatory B subunit (42). We found that MC3T3-E1 cells are not PTH-responsive (data not shown), and therefore sought to determine phosphatase involvement in primary calvarial osteoblasts. Okadaic acid is a commonly used inhibitor of PP1/PP2A, and inhibition of either or both phosphatases can be determined by using two different concentrations (PP2A: IC_{50} 0.02–0.5 nM PP1: IC_{50} 10–200 nM). Inhibition of PP2A by 50 nM okadaic acid (OA) decreased basal levels of *Rankl* by 75% and attenuated the effects of PTH(1–34), PTHrP(1–36), and ABL by 50, 55, and 80%, respectively. Inhibition of both Ser/Thr phosphatases, PP1 and PP2A by 200 nM OA decreased basal

Figure 1. PTHrP(1–36) and ABL are weaker activators of cAMP/PKA/CREB signaling compared with PTH(1–34). *a,* cAMP stimulation. Primary calvarial osteoblasts were treated with 750 nM peptides at the indicated times. Cells were lysed in buffer containing 2 mM IBMX. cAMP detection was performed by ELISA and readings were calculated against a cAMP standard curve as described under "Experimental procedures." Groups with dissimilar letters signify $p < 0.05$. Compared with PTH(1–34), PTHrP (1–36) values at 10, 20, and 30 min are $p < 0.05$. All ABL values in *panel a* are $p < 0.05$ compared with all the other groups. Area-under-the-curve values for PTH(1–34) were 11,971 (S.D. = 710.4); PTHrP(1–36), 9,253 (S.D. = 816.8); and ABL, 2,036 (S.D. = 309.9). All groups are $p < 0.05$ compared with each other. *b* and *c,* PKA activation. Primary calvarial osteoblasts were treated with (*b*) 10 nM peptides for up to 5 min or (*c*) with the indicated concentrations for 1 min prior to lysis. Relative PKA activity is expressed as a ratio of phosphorylated PKA substrate over total substrate. *d* and *e,* CREB phosphorylation. Primary calvarial osteoblasts were treated with (*d*) 10 nM peptides from 1 to 60 min or (*e*) with the indicated doses for 5 min prior to whole cell lysis and immunoblotting. Samples were quantified using Bio-Rad ImageLab software and calculated against the total detectable protein per lane. All data represent the mean ± S.D. of $n = 3$ independent experiments and images are representative of mean results.

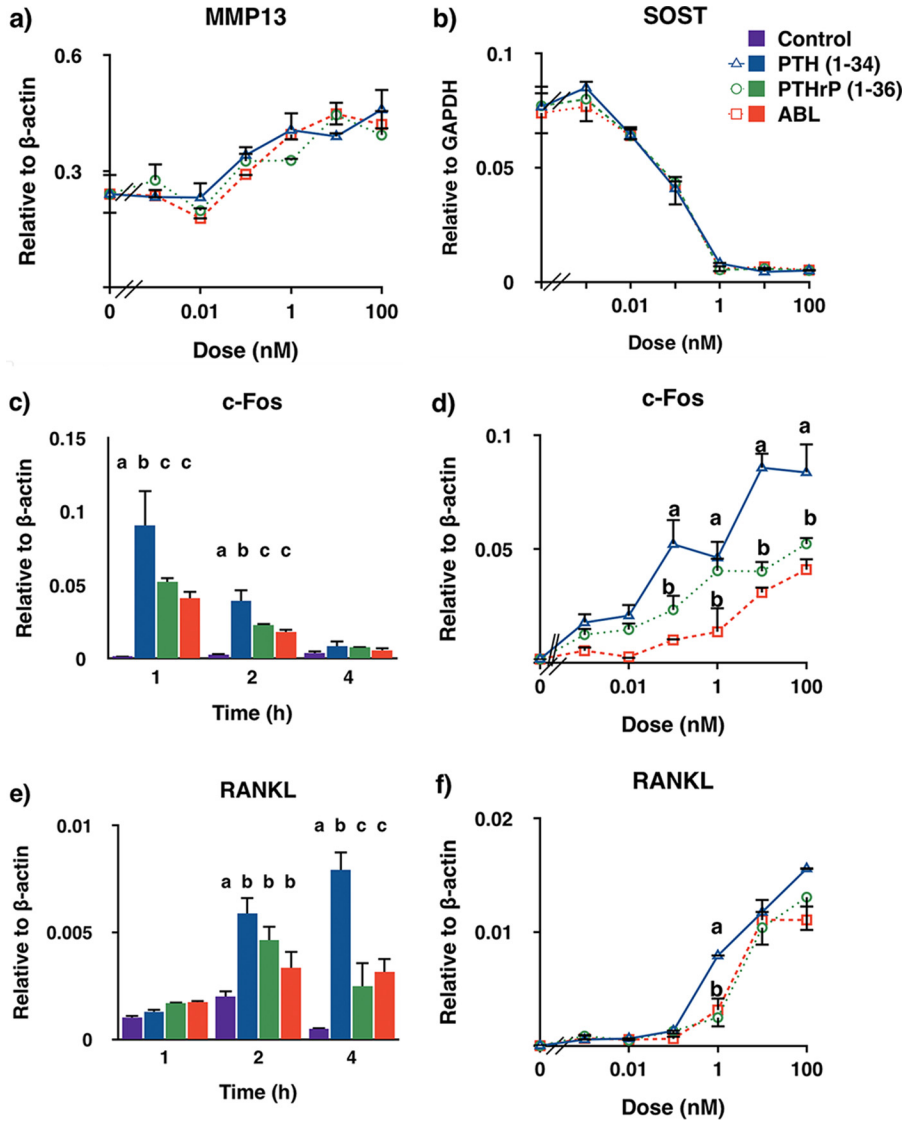

Figure 2. PTH(1–34), PTHrP(1–36), and ABL differentially regulate c-*Fos* and *Rankl* mRNA. *a, Mmp13* mRNA. Primary calvarial osteoblasts were treated for 4 h with 0.001 to 100 nM peptides, followed by qRT-PCR analysis for *Mmp13* mRNA. *b, Sost* mRNA. UMR 106-01 cells were treated for 4 h with 0.001 to 100 nM peptides, followed by qRT-PCR analysis for *Sost* mRNA. *c* and *d,* c-*Fos* mRNA. Primary calvarial osteoblasts were treated with (*c*) 100 nM peptides for 1 or 4 h, or (*d*) at 1 h with doses ranging from 0.001 to 100 nM, followed by qRT-PCR for c-*Fos* mRNA. *e* and *f, Rankl* mRNA. Primary calvarial osteoblasts were treated with (*e*) 1 nM peptides for 1, 2, or 4 h, or (*f*) at 4 h with doses ranging from 0.001 to 100 nM, followed by qRT-PCR for *Rankl* mRNA. All data are expressed relative to housekeeping genes *β-actin* or *Gapdh* and represent the mean ± S.D. of $n = 3$ independent experiments. Groups with dissimilar letters signify $p < 0.05$. For *Mmp13* mRNA, 1 to 100 nM doses are $p < 0.05$ compared with their respective 0 dose. For *Sost* mRNA, 0.1 to 100 nM doses are $p < 0.05$ compared with their respective 0 dose.

levels of *Rankl* by 64% and decreased the effects of PTH(1–34), PTHrP(1–36), and ABL by 93, 59, and 75%, respectively (Fig. 3*b*). Adenoviral-mediated expression of the PP2A-specific inhibitor, SV40 small T-antigen, attenuated the effects of all peptides by 60–70% (Fig. 3*c*), and abolished any differential effects between the peptides, implicating PP2A as a phosphatase that plays a major role in the regulation of *Rankl* mRNA expression. Nevertheless, PP1 may also be involved. These data show that cAMP/PKA and PP1/PP2A signaling is required for maximal osteoblastic *Rankl* expression.

Differential regulation of Rankl is observed in vivo and in a PKA-dependent fashion

To corroborate our data *in vivo*, we injected 4-month-old male C57Bl/6 WT mice with 80 μg/kg/day of vehicle or peptides for 6 weeks and harvested tibial shafts to enrich for RNA derived from osteoblast/osteocyte-rich cortical bone. We found that PTH(1–34) injections led to a 3-fold increase in *Rankl*, whereas PTHrP(1–36) and ABL only resulted in a 1.5-fold increase (Fig. 3*d*). To examine the effects of PKA up-regulation *in vivo*, we deleted the regulatory subunit of PKA (PRKAR1a) in osteoblasts by crossing *Col1*-Cre-ER^{T} mice with *Prkar1a*$^{fl/fl}$ mice and induced deletion by tamoxifen injections. Four-week-old male and female mice were injected for 3 weeks and 5-month-old mice were injected once a week for 4 weeks prior to tissue harvest. We observed an increase in *Rankl* mRNA of 2.8-fold in 7-week-old female mice and 4-fold in male mice (Fig. 3*e*). We also observed a 5-fold increase of *Rankl* mRNA in 6-month-old mice (Fig. 3*f*). Taken together, the *in vivo* findings corroborate the results seen in primary cultured

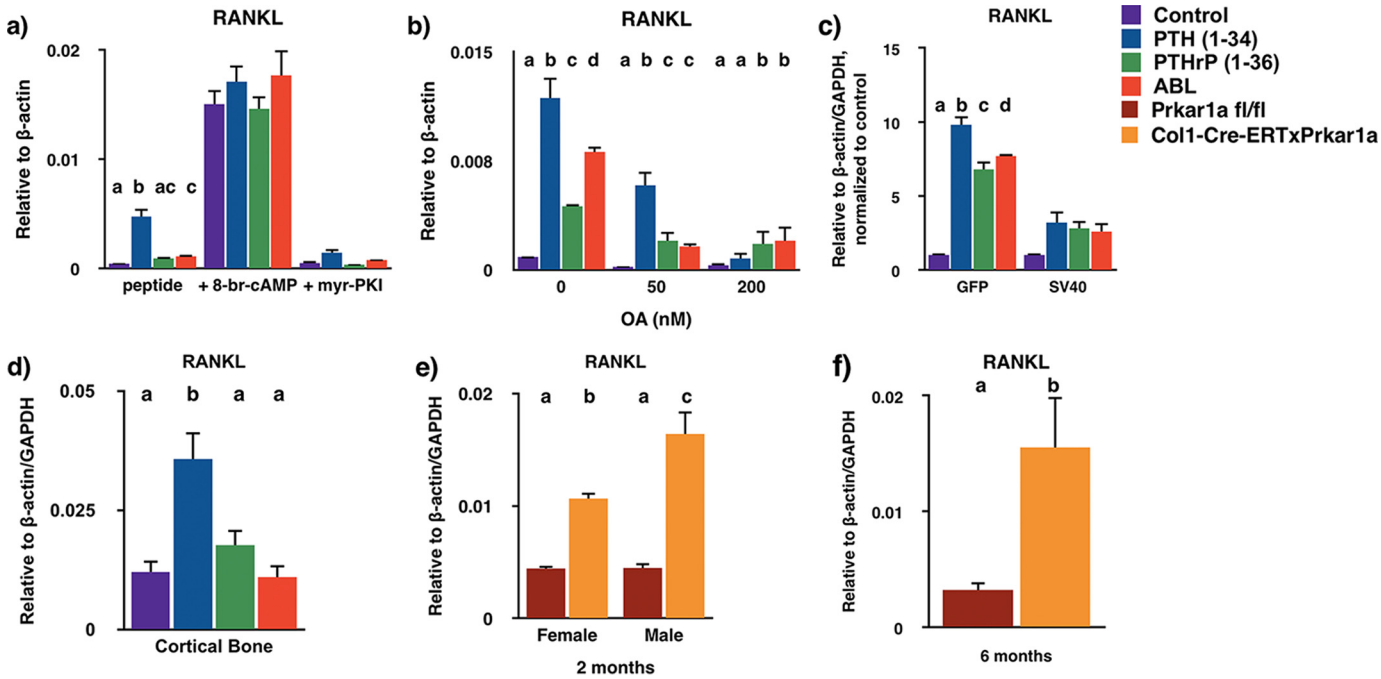

Figure 3. Differential regulation of *Rankl in vivo* and *in* vitro utilizes the cAMP/PKA and PP1/PP2A signaling axis. *a*, primary calvarial osteoblasts were pre-treated for 30 min with 1 mM 8-Br-cAMP or for 4 h with 15 μM myr-PKI prior to 1 nM peptides for 4 h. Data are expressed relative to the housekeeping gene *β-actin*. *b,* primary calvarial osteoblasts were pre-treated with 50 or 200 nM OA for 2 h prior to 4 h treatment with 1 nM peptides (1–34). Data are expressed relative to the housekeeping gene *β-actin*. *c,* primary calvarial osteoblasts were transfected overnight with adenoviral SV40 small T-antigen or GFP empty vector. Subsequently, cells were treated with 10 nM peptides for 4 h. Data are expressed relative to the housekeeping genes *β-actin* and *Gapdh*, normalized to each control, and represent the mean ± S.E. of $n = 3$ independent experiments. *d,* 16-week-old C57Bl/6 WT male mice were given 80 μg/kg/day of vehicle or peptides for 6 weeks ($n = 10$/group). Eighteen h after the final injections, tibial shaft mRNA was harvested and processed for qRT-PCR. Data are expressed relative to the housekeeping genes *β-actin* and *Gapdh* and represent the mean ± S.E. *e,* 4-week-old *Prkar1a*$^{fl/fl}$ or *Col1-Cre*-ER^{T}x/*Prkar1a*$^{fl/fl}$ mice were injected with 1 mg of tamoxifen/animal once a week for 3 weeks prior to tibial harvest for qRT-PCR (females: $n = 10$ *Prkar1a*$^{fl/fl}$, $n = 8$ *Col1*-Cre-ER^{T}x/*Prkar1a*$^{fl/fl}$; males: $n = 10$ *Prkar1a*$^{fl/fl}$, $n = 9$ *Col1*-Cre/ER^{T}x/*Prkar1a*$^{fl/fl}$). *f,* 6-month-old male *Prkar1a*$^{fl/fl}$ or *Col1*-Cre-ER^{T}x/*Prkar1a*$^{fl/fl}$ mice were injected with 2.5 mg of tamoxifen/animal once a week for 4 weeks prior to tibial harvest for qRT-PCR ($n = 4$ *Prkar1a*$^{fl/fl}$, $n = 7$ *Col1*-Cre-ER^{T}x/*Prkar1a*$^{fl/fl}$). *Prkar1a*$^{fl/fl}$ mice were used as control and data are expressed relative to the housekeeping genes *β-actin* and *Gapdh* and represent the mean ± S.E. Groups with dissimilar letters signify $p < 0.05$.

osteoblasts. Additionally, activation of PKA *in vivo* alone is able to drive *Rankl* expression to a greater degree than PTH(1–34).

Osteoblastic Rankl expression depends on SIK2/SIK3 and CRTC3

Previous studies had reported that PTH-induced osteoblastic *Rankl* expression depended on the PKA-dependent phosphorylation of HDAC4 and its dissociation from the transcription factor, MEF2c (43). Surprisingly, we found that siRNA-mediated knockdown of either HDAC4 or MEF2c did not abrogate the effect of PTH(1–34) on *Rankl* mRNA expression (Fig. S2). Recently, SIKs have been shown to be prominent effectors of osteocytic *Rankl* and *Sost* expression. PTH has been shown to promote the PKA-dependent inhibitory phosphorylation of SIK2 and SIK3, which in turn, decreases the tonic phosphorylation of CREB-regulated transcription coactivator, CRTC2. CRTC2 dephosphorylation leads to its dissociation from 14-3-3 cytoplasmic proteins and allows its nuclear translocation and subsequent association with a bZIP transcription factor at the −75 kb enhancer region of the *Rankl* promoter (23). In primary osteoblasts, knockdown of SIK2 and SIK3 results in a 5-fold increase in basal *Rankl* mRNA levels, and a 2–3–fold increase in the effects of all peptides (Fig. 4*a*). Interestingly, knockdown of CRTC2 or CREB did not significantly alter the basal levels of *Rankl* mRNA or the effects of PTH(1–34), PTHrP(1–36), or ABL (Fig. 4*b*), implying that PKA signaling modulates osteoblastic *Rankl* expression through other effectors. However, knockdown of CRTC3 decreased basal RANKL mRNA levels by 50%, and reduced the effects of all peptides by 30% (Fig. 4*c*). This suggests that SIK2, SIK3, and CRTC3 play an important role in osteoblastic *Rankl* expression, and that CRTC2 and/or CRTC3 do not require CREB, but presumably bind other transcription factors containing bZIP domains on the *Rankl* promoter.

Compared with PTH(1–34), PTHrP(1–36), and ABL lead to less nuclear translocation of CRTC2 and CRTC3

SIKs have been shown to be directly inhibited by cAMP/PKA activity (44) and their direct targets (CRTC family members) are regulated by phosphorylation-dependent nuclear-cytoplasmic shuttling (24). We and others have shown that CRTC2 and CRTC3 are involved in osteocytic/osteoblastic *Rankl* expression. Therefore, we hypothesized that PTH(1–34), PTHrP(1–36), and ABL would differentially regulate nuclear/cytoplasmic CRTC2/CRTC3 distribution in osteoblasts. After 60 min of treatment, PTH(1–34) resulted in the highest proportion of nuclear-localized CRTC2 (70%) and CRTC3 (79%), whereas PTHrP(1–36) resulted in lower CRTC2 (38%) and CRTC3 (48%) nuclear localization, and also ABL (CRTC2 = 40%, CRTC3 = 46%, Fig. 5, *a* and *b*). These results mirror the relative effects of PTH(1–34), PTHrP(1–36), and ABL on cAMP/PKA signaling and suggest that compared with PTH(1–34), the

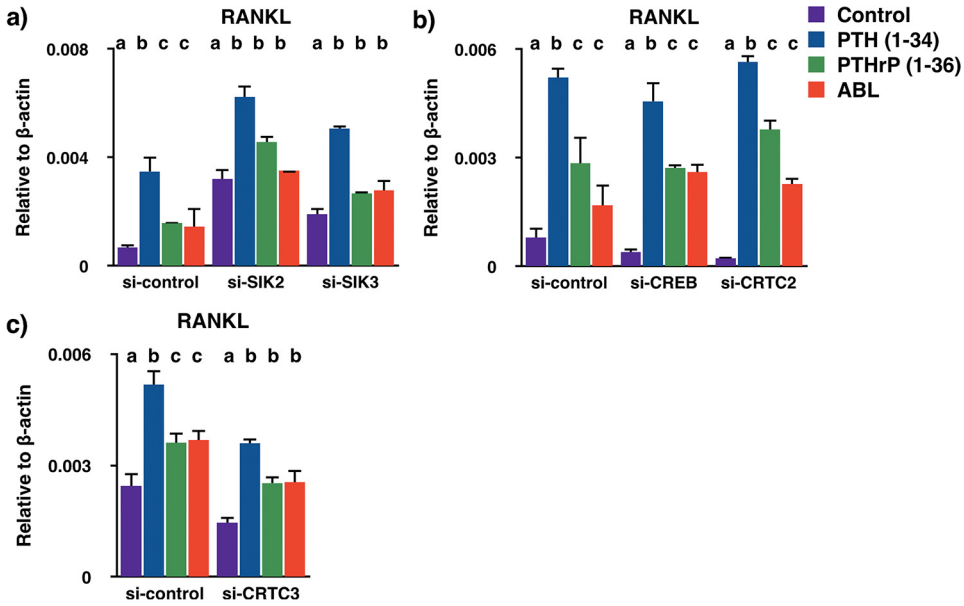

Figure 4. SIK2/SIK3 and CRTC3 modulate osteoblastic *Rankl* expression. *a–c*, primary calvarial osteoblasts were transfected with 1 μM (*a*) control siRNA, si-SIK2, si-SIK3, (*b*) si-CREB, si-CRTC2, or (*c*) si-CRTC3 for 72 h prior to 1 nM peptides for 4 h, followed by qRT-PCR for *Rankl* mRNA. Data are expressed relative to the housekeeping gene *β-actin* and represent the mean ± S.D. of $n = 3$ independent experiments. Groups with dissimilar letters signify $p < 0.05$.

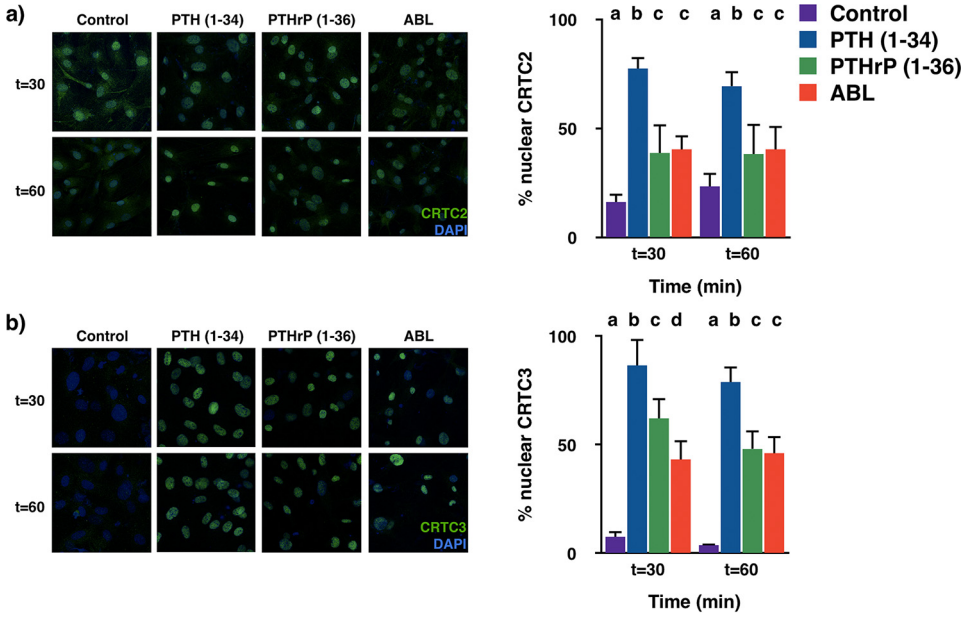

Figure 5. PTHrP(1–36) and ABL lead to lower nuclear translocation of CRTC2/CRTC3 compared with PTH(1–34). Primary calvarial osteoblasts were treated with 50 nM peptides for 30 or 60 min and assayed for (*a*) CRTC2 and (*b*) CRTC3 localization by immunofluorescence. Quantitation of nuclear localization was performed on ImageJ and was measured by comparing intensities of the GFP signal overlaid onto nuclear DAPI signal. For each condition, $n = 500 \pm 50$ cells were counted and data represent the mean ± S.D. of $n = 3$ independent experiments. Images shown are representative of mean results. Groups with dissimilar letters signify $p < 0.05$.

decreased effects of PTHrP(1–36) and ABL on this particular signaling axis lead to a weaker inhibition of SIK2 and SIK3 and consequently, lesser nuclear localization of CRTC2 and CRTC3, which ultimately results in relatively lower levels of *Rankl* mRNA.

PTH-induced translocation of CRTC2 and CRTC3 requires SIK2 and PP1/PP2A

Because we found that PTH(1–34) and its analogs require SIKs 2 and 3, CRTC3, and PP1/PP2A to modulate *Rankl* mRNA expression, and all three peptides affect the nuclear translocation of CRTC2/CRTC3, we assessed the potential of PTH(1–34), the strongest of the three cAMP/PKA agonists, to regulate the localization of CRTC2 and CRTC3 in the absence of SIK2 and PP1/PP2A activity. siRNA-mediated SIK2 knockdown resulted in a 36% increase in basal levels of nuclear CRTC2, and enhanced the PTH(1–34)-induced nuclear translocation by 10% (Fig. 6*a*), thus confirming its inhibitory effect on CRTC2. Surprisingly, knockdown of SIK2 did not have any significant effects on basal levels of nuclear CRTC3, nor did it alter the

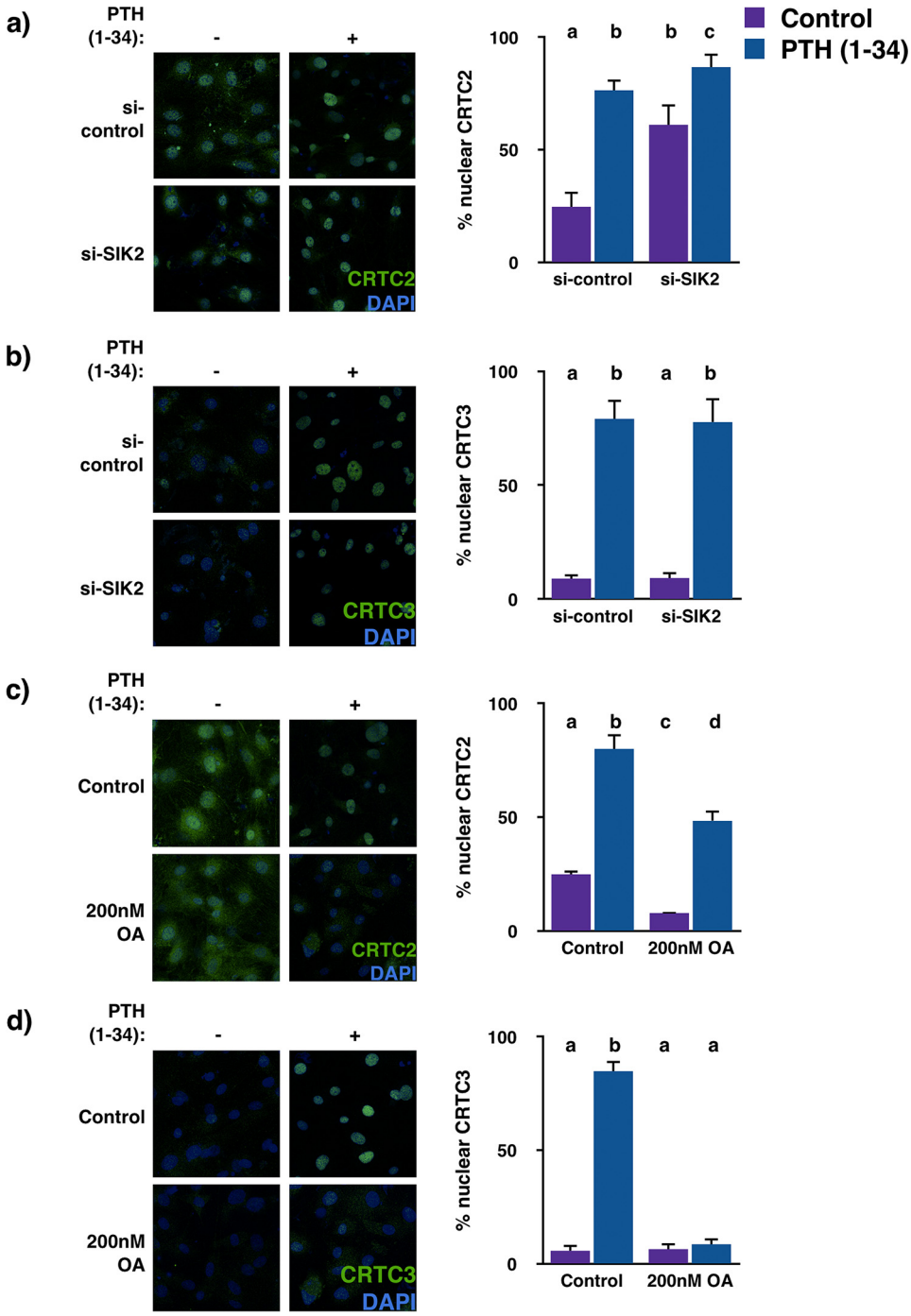

Figure 6. PTH(1–34) regulates CRTC2 and CRTC3 subcellular localization through SIK2 and PP1/PP2A, respectively. *a* and *b*, primary calvarial osteoblasts were transfected with 1 μM si-control or si-SIK2 for 72 h prior to 1 h treatment with 50 nM PTH(1–34). *c* and *d*, primary calvarial osteoblasts were pre-treated with 200 nM OA for 2 h prior to a 1 h treatment with 50 nM PTH(1–34). Cells were incubated with primary antibodies to detect (*a* and *c*) CRTC2 and (*b* and *d*) CRTC3 localization. Images were captured and analyzed as described in the legend to Fig. 5. For each condition, $n = 500 \pm 50$ cells were counted and data represent the mean $\pm$ S.D. of $n = 3$ independent experiments. Images shown are representative of mean results. Groups with dissimilar letters signify $p < 0.05$.

effects of PTH(1–34) (Fig. 6*b*). Inhibition of PP1/PP2A by 200 nM OA decreased basal levels of nuclear CRTC2 by 17%, and decreased the effects of PTH(1–34) by 32% (Fig. 6*c*). Additionally, PP1/PP2A inhibition did not alter basal levels of nuclear CRTC3, but dramatically decreased the effects of PTH(1–34) on CRTC3 localization by 76% (Fig. 6*d*). These data suggest that whereas both PP1/PP2A and SIK2 are responsible for CRTC2 localization, PP1/PP2A seem to play a more prominent role in controlling nuclear CRTC3 localization in PTH signaling.

Discussion

We have shown that whereas PTH(1–34), PTHrP(1–36), and ABL exert similar effects on a subset of genes (Table 2), PTHrP(1–36) and ABL appear to be weaker agonists of the cAMP/PKA/SIK2–SIK3/CRTC signaling axis, and this is par-

ticularly clear in the differential effects on *Rankl* mRNA, as well as in CRTC2/CRTC3 localization. Our *in vitro* binding data suggest that in osteosarcoma cells, ABL binding to PTHR1 is similar to PTH(1–34). Because the assay was performed on intact cells and without GTPγS, which, in assays performed in membranes, enriches for the G protein-uncoupled conformation (R^0) through inducing receptor-G protein dissociation (45), we were unable to distinguish between R^0 and R^G and further studies must be conducted to delineate this. Nevertheless, the binding of ABL was slightly weaker (~2-fold) than that of human PTH(1–34) and significantly weaker (~10-fold) than that of a rat PTH(1–34) analog, which suggests a relatively weaker overall affinity of ABL as compared with PTH ligands for the rat PTHR1 in the intact cell line. Although the differences we report with respect to the cAMP responses elicited by the peptides vary slightly from other reports (25), we believe that this is due to the nature of the cell types being studied. Our system employs primary calvarial osteoblasts, which express native levels of PTHR1. Nonetheless, we observed time and dose-dependent differences between all three peptides in their ability to activate PKA (Fig. 1, *b* and *c*), in addition to downstream activation of CREB (Fig. 1, *c* and *d*), which are both sequentially downstream of cAMP stimulation. Our data show that this pathway is titratable, as observed with PKA agonists and antagonists (Fig. 3*a*), and with the deletion of the PKA regulatory subunit *in vivo* (Fig. 3, *d* and *e*).

Because we observed weaker cAMP/PKA signaling by PTHrP(1–36) and ABL compared with PTH(1–34), and others have reported that this signaling accounts for the inhibitory effects of PTH on osteocyte *Sost* expression through SIK2/HDAC4/5/MEF2c (23), we expected to find differential inhibition of osteoblast *Sost* expression by all three peptides. Surprisingly, their inhibitory effects were identical and relatively sensitive in UMR 106-01 cells (Fig. 2*b*). We attempted to replicate this in primary calvarial osteoblasts, but basal *Sost* levels were much lower compared with UMR 106-01 cells and we were unable to observe any effects with PTH(1–34) (data not shown). Nonetheless, this finding suggests clear differences in the effects of all three peptides on the SIK/HDAC4/5/MEF2c and SIK/CRTC signaling axes, and that the former is more sensitive to changes in cAMP/PKA activity. Also, the equipotent effects of PTH(1–34), PTHrP(1–36), and ABL on *Sost* suppression may account for the equipotent effects observed *in vivo* (7). It is also interesting to note the differences between the effects of these peptides on *Sost* mRNA *versus Rankl* mRNA. The minimum dose required for an observable change in *Sost* mRNA was 0.1 nM (1/2 max = 0.085 nM), whereas the effects of all three peptides on RANKL mRNA were observable at 1 nM, and both effects are maximal at 4 h. Because the regulation of each gene requires transcriptional termination and activation for *Sost* and *Rankl*, respectively, it is conceivable that this indicates that transcriptional termination may require a weaker stimulus compared with transcriptional activation.

SIKs are direct downstream effectors of cAMP/PKA signaling and respond to metabolic changes in different systems (47–49). There appears to be redundancy between SIK2 and SIK3 (50), and we observed this in our system, because knockdown of either protein results in the modulation of *Rankl* mRNA (Fig. 4). Although knockdown of SIK2 yielded greater effects on *Rankl* mRNA compared with SIK3, SIK3 knockdown was still effective in increasing osteoblastic *Rankl* mRNA. Although SIK3 is not a reported downstream target of PTH signaling, SIK3 deficiency phenocopies PTHrP overexpression in chondrocytes, suggesting that it is somehow involved in the pathway (51, 52).

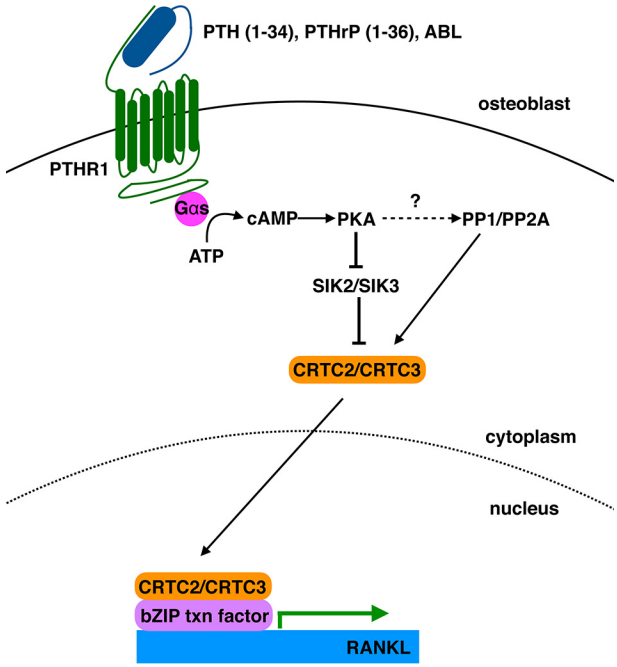

Figure 7. Working model of the effects of PTH(1–34), PTHrP(1–36), and ABL on SIK2/3 inhibition, PP1/PP2A activation, and nuclear translocation of CRTC3 in the osteoblast. In the osteoblast, PTH(1–34), PTHrP(1–36), and ABL have differential effects on cAMP stimulation and PKA activation. Nonetheless, PKA phosphorylates salt-inducible kinases SIK2 and SIK3, which lessens the inhibitory phosphorylation of CRTC3 by SIK2/SIK3. Concurrently, PP1/PP2A dephosphorylates CRTC3 and both events dissociate CRTC3 from 14-3-3 cytoplasmic proteins. CRTC3 enters the nucleus and binds an unknown bZIP transcription factor to enhance *Rankl* gene transcription.

Our results show that the effects of PTH(1–34) and its analogs differ in the primary osteoblast *versus* the osteocyte with respect to the regulation of *Rankl* (Fig. 7). Although others have reported that CRTC2 is the main cofactor involved in osteocytic *Rankl* expression (23), we report that PTH(1–34) and its analogs indeed affect CRTC2 localization, but CRTC3 appears to be the main effector in the osteoblast. Kim *et al.* (53) observed redundancy between CRTC2 and CRTC3 in bone marrow, because CRTC2/CRTC3 double knockout mice exhibited embryonic lethality, but only one allele of either CRTC2 or -3 was sufficient for viability. It is possible that there is redundancy between CRTC2 and CRTC3 in the osteoblast, and perhaps there may even be events in late osteoblast differentiation/maturation that generate a switch from CRTC3 to CRTC2 with respect to *Rankl* signaling. Simultaneous knockdown of CRTC2 and CRTC3 in the osteoblast would shed light on these open issues. However, this was attempted and the knockdown was not effective in primary calvarial osteoblasts (data not shown).

Several groups have implicated CREB in *Rankl* regulation through its upstream enhancers (17, 36, 54, 55). Interestingly, we have shown that the CREB coactivator, CRTC3, plays a role

in enhancing *Rankl* up-regulation, but knockdown of CREB did not hinder the effects of PTH(1–34) or the other peptides on *Rankl* mRNA (Fig. 4, *b* and *c*). We postulate that other transcription factors with bZIP domains are able to bind the CRTCs at the −75 kb enhancer region, but further studies must be conducted to determine this.

Our data implicate PP1 and PP2A as important mediators of PKA signaling in PTH-stimulated osteoblasts. Indeed, inhibition of PP1/PP2A by okadaic acid significantly altered the effects of PTH(1–34) on both *Rankl* mRNA (Fig. 3*b*) and CRTC2 and -3 localization (Fig. 6, *c* and *d*), but inhibition of PP2A by SV40 small T-antigen was sufficient to attenuate the effects of all peptides on *Rankl* mRNA (Fig. 3*c*). Thus, we hypothesize that PP2A is the main Ser/Thr phosphatase involved in PTH signaling. Additionally, pre-treatment with the PP2A agonist, FTY720, was able to increase *Rankl* mRNA 2-fold (data not shown). It has previously been shown that PKA phosphorylates three Ser residues on the PP2A subunit, B″, and that this promotes PP2A activity (56). Further studies *in vitro* using HEK293 cells and *in vivo*, in striatal neurons, revealed that PKA phosphorylates the PP2A subunit, B56δ, and this leads to the up-regulation of PP2A activity (57). In another study using NRK-52E and L6 cells, cAMP up-regulation by forskolin and isobutylmethylxanthine (IBMX) led to decreased phosphorylation of PP2A substrate, elongation factor-2 and these dephosphorylation events were blocked by PP2A inhibition with okadaic acid. However, inhibition of PKA with H-89 did not block cAMP-dependent dephosphorylation, suggesting that the pathway of PP2A activation in these cells is cAMP-dependent, but PKA-independent (58). The complexity of its regulation leaves many open questions about the mechanism of osteoblastic PP2A activation and substrate (CRTC3) recognition, which require further investigation. Although calcineurin (or protein phosphatase 3) was implicated in CRTC dephosphorylation (59), our experiments with OA and SV40 small T-antigen support a role for PP2A in the PTH-induced nuclear translocation of CRTC2 and CRTC3, in addition to the regulation of *Rankl* mRNA expression (Figs. 3, *b* and *c*, and 6, *c* and *d*). However, inhibition of calcineurin with cyclosporine in primary calvarial osteoblasts would definitively rule out this possibility. Whether or not PP2A directly dephosphorylates CRTC2 and CRTC3 or another substrate (perhaps SIK2 and SIK3) remains to be seen. We hypothesize that PP1/PP2A dephosphorylates CRTCs 2 and 3, because PP1/PP2A inhibition decreased the effects of PTH(1–34) on CRTC2 nuclear localization (Fig. 6*c*) and potently inhibited its effects on CRTC3 localization (Fig. 6*d*), whereas the effects of SIK2 knockdown were milder. Interestingly, SIK2 knockdown had greater effects on CRTC2 and no effects on CRTC3, which may suggest one of two possibilities: there is an alternative mode of signaling outside of the SIK axis that governs PTH-induced CRTC2 and CRTC3 nuclear localization, or the dephosphorylation of CRTCs plays a more pivotal role in modulating its subcellular localization. SIK2 and PP2A have been shown to interact with each other, and increases in cAMP/PKA activity disrupt this association (47). Others have also shown that this SIK2-PP2A binding acts to preserve the activity of each enzyme to regulate calcium/calmodulin-dependent Protein Kinase I (60). However, we have shown that in the osteoblast, inhibition of PP1/PP2A did not weaken SIK2 activity, as this would have resulted in increased CRTC localization and *Rankl* mRNA expression, whereas we observed the opposite (Fig. 6, *c* and *d*). Others have shown that in MC3T3-E1 cells, inhibition of PP2A-Cα by short hairpin RNA decreased *Rankl* mRNA, but also increased osteoprotegerin mRNA (41). The same group also observed an increase in osteoblastic transcription factors, *Osterix*, *bone sialoprotein*, and *Osteocalcin*, upon inhibition of PP2A by 1 nM okadaic acid (46). Concurrent with our findings, these data suggest a major role for PP2A in osteoblastic signaling and, particularly, in the regulation of *Rankl* expression. In this study, we have shown titratable differences between PTH(1–34), PTHrP(1–36), and ABL on cAMP/PKA signaling in the osteoblast. Our study provides greater insight into how these peptides exert their effects and may provide a deeper understanding as to how their differences are achieved *in vivo*.

Experimental procedures

Peptides and chemicals

Rat parathyroid hormone (PTH(1–34)) was purchased from Sigma. Parathyroid hormone-related protein (PTHrP(1–36)) and ABL were custom synthesized by the Peptide/Protein Core Facility at the Massachusetts General Hospital. Human PTH(1–34) was purchased from Bachem. Additionally, a second preparation of PTHrP(1–36) and ABL were custom synthesized by Bachem. All PTH(1–34), PTHrP(1–36), and ABL peptide sequences were confirmed and analyzed for purity and degradation by the New York University Langone Mass Spectrometry Core Facility. RIPA buffer, 8-bromo-cAMP, and ascorbic acid were purchased from Sigma. Collagenase A was purchased from Worthington Biochemical Corp. Myr-PKI was purchased from Tocris. IBMX was purchased from MP Biomedicals. Paraformaldehyde was purchased from EM Sciences. For binding assays, C-terminal amides were synthesized by the Peptide Core Facility at the Massachusetts General Hospital using conventional Fmoc (*N*-(9-fluorenyl)methoxycarbonyl)-based solid-phase chemistry and reverse phase-HPLC on a prep-C18 column for purification. Purity (>95) and molecular mass were established by analytical RP-HPLC and MALDI-TOF-MS.

Antibodies

See Table S2 for a full list of primary antibodies and concentrations. Goat anti-rabbit horseradish peroxidase (HRP)-linked secondary antibody was purchased from Cell Signaling Technologies. Donkey anti-rabbit Alexa Fluor 488 secondary antibody was purchased from Life Technologies.

Cell culture

Rat osteoblastic, osteosarcoma cell line, UMR 106-01, was cultured using Eagle's minimal essential medium, supplemented with 5% fetal bovine serum (FBS), 25 mM HEPES, 1% nonessential amino acids, 100 units/ml of penicillin, and 100 μg/ml of streptomycin. Primary calvarial osteoblasts were harvested from C57Bl/6 WT mice aged 2–5 days postnatal. Mice were euthanized with ketamine and xylazine (0.5 mg and 0.025 mg/pup, respectively). Calvariae were digested in 1 mg/ml of

collagenase A at 37 °C by five sequential digestions, and cells from digests 3–5 were collected and plated at a density of 6.4×10^3 cells/cm^2 in αMEM supplemented with 10% FBS and 100 units/ml of penicillin and 100 μg/ml of streptomycin. After reaching confluence, osteogenic medium (50 μg/ml of ascorbic acid) was added for 3 days to allow osteoblastic differentiation. Primary bone cells were harvested using femoral chips from 3-month-old male C57BL/6 WT mice. Cells were cultured to confluence and after the first plating, were treated similarly to primary calvarial osteoblasts. The osteoblastic phenotype of all primary cells was confirmed by measuring the relative mRNA levels of osteoblastic genes, *Col1a1* and *Alp*. For all experiments, cells were serum-starved with 0.1% FBS 24 h prior to peptide treatments.

In vivo study design

All experiments using mice were performed following protocols approved by the New York University Institutional Animal Care and Use Committee (IACUC). Intermittent subcutaneous peptide injections of 80 μg/kg/day were administered to 4-month-old C57Bl/6 male mice for 6 weeks ($n = 10$/group). Eighteen h after the final injection, tibial shafts were harvested and processed for qRT-PCR analyses. Additionally, 4-week-old *Col1*-Cre-ER^T/*Prkar1a*$^{fl/fl}$ mice (male: $n = 9$, female: $n = 8$) were injected with 1 mg of tamoxifen/mouse once a week for 3 weeks and 5-month-old *Col1*-Cre-ER^T/*Prkar1a*$^{fl/fl}$ mice ($n = 7$) were injected with 2.5 mg of tamoxifen once a week for 4 weeks prior to tibial mRNA harvest. *Prkar1a*$^{fl/fl}$ mice injected with tamoxifen were used as controls.

In vitro binding assays

Ligand binding to the rat PTHR1 in intact UMR 106 cells was assessed by competition methods using [^{125}I-Nle^{8,21},Tyr^{34}]rat PTH(1–34) as a tracer radioligand (2.2 Ci/mmol). Assays were performed in 96-well plates containing confluent cell monolayers in a buffer of Hanks' balanced salts solution supplemented with 10 mM HEPES, pH 7.4, and 0.1% BSA. Reactions contained radioligand (30,000 cpm/well) and varying concentrations of an unlabeled ligand, and were incubated at 4 °C for 17 h. The wells were then rinsed three times with cold buffer, lysed with 1 N NaOH, and the lysate was counted for γ-irradiation. Data from 4 independent experiments, each with either 3 replicates per dose-point (1 plate, $n = 2$) or 6 replicates per dose-point (2 plates, $n = 2$) were combined and plotted by fitting to a sigmoidal dose-response model with variable slope, such that each data point is an average (±S.E.) of values from 4 independent experiments. Reported pIC_{50} values are the averages (±S.E.) of the values obtained for each peptide in each of the 4 experiments.

In vitro cAMP and PKA assays

cAMP concentrations were measured using a cAMP XP assay kit and performed as described by the manufacturer (Cell Signaling). Briefly, cells were plated in triplicate in 96-well plates and cultured as described above. Following peptide treatments using αMEM supplemented with 0.1% FBS, the cells were washed in warm 1× PBS and lysed with 100 μl of lysis buffer (20 mM Tris-HCl, pH 7.5, 150 mM NaCl, 1 mM Na_2EDTA, 1 mM EGTA, 1% Triton, 2.5 mM sodium pyrophosphate, 1 mM β-glycerophosphate, 1 mM Na_3VO_4, 1 μg/ml of leupeptin) supplemented with 2 mM IBMX. Fifty μl were transferred into microtiter plates coated with anti-cAMP rabbit mAb. HRP substrate TMB was added to develop color, spectrophotometry measurements were taken at 405 nM, and readings were calculated against a cAMP standard curve. For PKA assays, cells were plated in triplicate in 6-well dishes and cultured as described above. PKA activity was measured using a PepTag nonradioactive protein kinase A assay and performed as described by the manufacturer (Promega). Following peptide treatments using αMEM supplemented with 0.1% FBS, the cells were washed in warm 1× PBS, scraped, and lysed in a Dounce homogenizer with 200 μl of PKA extraction buffer (25 mM Tris-HCl, pH 7.4, 0.5 mM EDTA, 0.5 mM EGTA, 10 mM β-mercaptoethanol, 1 μg/ml of leupeptin, 1 μg/ml of aprotinin) and 10 μl were incubated with PKA reaction buffer and Peptag A1 Peptide PKA substrate (P-L-S-R-T-L-S-V-A-A-K). Samples were processed in 1% agarose gels and imaged with Bio-Rad gel documentation system for densitometric detection of PKA substrates. Samples were analyzed by measuring the ratio between phosphorylated PKA substrates over total PKA substrates.

siRNA knockdown

si-control, si-SIK2, si-SIK3, si-CRTC2, si-CRTC3, si-CREB, si-HDAC4, and si-MEF2c Accell siRNA reagents were purchased from Dharmacon and transfection was performed as described by the manufacturer. Briefly, siRNA was diluted to a final concentration of 1 μM with αMEM supplemented with 2.5% fetal bovine serum (FBS) and incubated at 37 °C for 1 h. siRNA media were then added to cells and incubated for 72 h prior to peptide treatments. Confirmation of knockdowns was confirmed by Western blotting or RNA (Fig. S3).

Adenoviral infection

For adenoviral infection, primary calvarial osteoblasts were plated as described above. Cells were exposed to 10 pfu/cell of Ad-SV40 small T antigen overnight at 37 °C. The following morning, cells were serum-starved in αMEM supplemented with 0.1% FBS for 4 h prior to peptide treatments.

qRT-PCR

Total RNA was extracted using TRIzol (Sigma). Complementary DNA (cDNA) was synthesized from 1 μg of total RNA using a TaqMan reverse transcription kit (Applied Biosystems) with hexamer primers following the protocol described by the manufacturer. Gene expression levels were measured using SYBR Green PCR reagents (Applied Biosystems). Primer pairs used for quantitative detection of gene expression are listed in Table S1. The quantity of mRNA was calculated by normalizing the threshold cycle value (C_t) of specific genes to the C_t of the housekeeping gene *β-actin* and/or glyceraldehyde-3-phosphate dehydrogenase (*Gapdh*).

Western blotting

Whole cell lysates were prepared using RIPA buffer (150 mM NaCl, 1% IGEPAL, 0.5% sodium deoxycholate, 0.1% SDS, 50 mM Tris, pH 8.0; Sigma) supplemented with 1× HALT protease and phosphatase inhibitor cocktails (Thermo). Total protein

concentration was determined by Bradford reagents (Bio-Rad). Twenty μg of lysates were resolved on TGX Stain-free SDS-polyacrylamide gels and transferred onto polyvinylidene fluoride membranes using the Trans-Blot Turbo Transfer system (Bio-Rad). Prior to immunoblotting, membranes were imaged to detect total protein content as described by the manufacturer. Membranes were blocked with 5% nonfat milk in TBST, and incubated overnight with primary antibodies. Subsequently, membranes were washed, incubated with HRP-linked secondary antibodies, and signals were detected by chemiluminescence (Pierce). Blots were imaged and quantified using Bio-Rad ImageLab software and calculated against total detectable protein per lane.

Immunofluorescence

Cells were fixed with 3.7% paraformaldehyde and 0.002% Triton X-100 for 30 min and blocked with 1% BSA in 1× PBS for 1 h. Cells were incubated with 1:250 dilution of primary antibodies for 1 h, followed by washes and incubation with 1:450 dilution of Alexa Fluor 488-conjugated secondary antibodies. Cells were incubated with 1:10,000 DAPI (Life Technologies) for nuclear staining and mounted using Fluoromount-G fluorescence mounting medium (Invitrogen). Images were captured with a Zeiss LSM 700 laser scanning confocal microscope and automated quantitation of nuclear localization was performed on ImageJ and measured by comparing intensities of GFP signal overlaid onto nuclear 4′,6-diamidino-2-phenylindole (DAPI) signal. For each condition, $n = 500 \pm 50$ cells were counted for statistical analysis.

Statistics

All experiments were performed at least three times and in triplicate per experiment. Statistical differences were analyzed either by Student's t test, or one-way or two-way analysis of variance using IBM SPSS (v24). Results are expressed as mean ± S.D. or S.E. and a $p < 0.05$ was considered significant comparing treatment groups.

Author contributions—F. R. R. and N. C. P. conceptualization; F. R. R., C. L. H., T. J. G., and N. C. P. data curation; F. R. R., C. L. H., T. J. G., and N. C. P. formal analysis; F. R. R., C. L. H., T. J. G., and N. C. P. validation; F. R. R., C. L. H., V. G. K., T. J. G., and N. C. P. investigation; F. R. R. and N. C. P. visualization; F. R. R., C. L. H., V. G. K., T. J. G., and N. C. P. methodology; F. R. R. and N. C. P. writing-original draft; C. L. H., V. G. K., T. J. G., and N. C. P. writing-review and editing; V. G. K., T. J. G., and N. C. P. resources; N. C. P. supervision; N. C. P. funding acquisition; N. C. P. project administration.

Acknowledgments—We thank Dr. Henry Kronenberg for providing Col1-Cre-ER^T mice, Dr. Lawrence Kirschner for providing Prkar1a$^{fl/fl}$ mice, and both for reading of the manuscript and helpful advice. We acknowledge Dr. Malvin Janal for guidance with statistical analyses, and Dr. Marc Wein for helpful advice and insight.

References

1. Harvey, N., Dennison, E., and Cooper, C. (2010) Osteoporosis: impact on health and economics. *Nat. Rev. Rheumatol.* **6,** 99–105 CrossRef Medline
2. Neer, R. M., Arnaud, C. D., Zanchetta, J. R., Prince, R., Gaich, G. A., Reginster, J. Y., Hodsman, A. B., Eriksen, E. F., Ish-Shalom, S., Genant, H. K., Wang, O., and Mitlak, B. H. (2001) Effect of parathyroid hormone (1–34) on fractures and bone mineral density in postmenopausal women with osteoporosis. *N. Engl. J. Med.* **344,** 1434–1441 CrossRef Medline
3. Hodsman, A. B., Bauer, D. C., Dempster, D. W., Dian, L., Hanley, D. A., Harris, S. T., Kendler, D. L., McClung, M. R., Miller, P. D., Olszynski, W. P., Orwoll, E., and Yuen, C. K. (2005) Parathyroid hormone and teriparatide for the treatment of osteoporosis: a review of the evidence and suggested guidelines for its use. *Endocr. Rev.* **26,** 688–703 CrossRef Medline
4. Rosen, C. J., and Bilezikian, J. P. (2001) Clinical review 123: Anabolic therapy for osteoporosis. *J. Clin. Endocrinol. Metab.* **86,** 957–964 CrossRef Medline
5. Kraenzlin, M. E., and Meier, C. (2011) Parathyroid hormone analogues in the treatment of osteoporosis. *Nat. Rev. Endocrinol.* **7,** 647–656 CrossRef Medline
6. Baron, R., and Hesse, E. (2012) Update on bone anabolics in osteoporosis treatment: rationale, current status, and perspectives. *J. Clin. Endocrinol. Metab.* **97,** 311–325 CrossRef Medline
7. Miller, P. D., Hattersley, G., Riis, B. J., Williams, G. C., Lau, E., Russo, L. A., Alexandersen, P., Zerbini, C. A., Hu, M. Y., Harris, A. G., Fitzpatrick, L. A., Cosman, F., Christiansen, C., and ACTIVE Study Investigators. (2016) Effect of abaloparatide vs placebo on new vertebral fractures in postmenopausal women with osteoporosis: a randomized clinical trial. *JAMA* **316,** 722–733 CrossRef Medline
8. Varela, A., Chouinard, L., Lesage, E., Guldberg, R., Smith, S. Y., Kostenuik, P. J., and Hattersley, G. (2017) One year of abaloparatide, a selective peptide activator of the PTH1 receptor, increased bone mass and strength in ovariectomized rats. *Bone* **95,** 143–150 CrossRef Medline
9. Doyle, N., Varela, A., Haile, S., Guldberg, R., Kostenuik, P. J., Ominsky, M. S., Smith, S. Y., and Hattersley, G. (2018) Abaloparatide, a novel PTH receptor agonist, increased bone mass and strength in ovariectomized cynomolgus monkeys by increasing bone formation without increasing bone resorption. *Osteoporos. Int.* **29,** 685–697 CrossRef Medline
10. Ureña, P., Kong, X. F., Abou-Samra, A. B., Juppner, H., Kronenberg, H. M., Potts, J. T., Jr., and Segre, G. V. (1993) Parathyroid hormone (PTH)/PTH-related peptide receptor messenger ribonucleic acids are widely distributed in rat tissues. *Endocrinology* **133,** 617–623 CrossRef Medline
11. Gardella, T. J., and Vilardaga, J. P. (2015) International Union of Basic and Clinical Pharmacology: XCIII. the parathyroid hormone receptors–family B G protein–coupled receptors. *Pharmacol. Rev.* **67,** 310–337 CrossRef Medline
12. Yang, D., Singh, R., Divieti, P., Guo, J., Bouxsein, M. L., and Bringhurst, F. R. (2007) Contributions of parathyroid hormone (PTH)/PTH-related peptide receptor signaling pathways to the anabolic effect of PTH on bone. *Bone* **40,** 1453–1461 CrossRef Medline
13. Cheloha, R. W., Gellman, S. H., Vilardaga, J. P., and Gardella, T. J. (2015) PTH receptor-1 signalling-mechanistic insights and therapeutic prospects. *Nat. Rev. Endocrinol.* **11,** 712–724 CrossRef Medline
14. Li, X., Liu, H., Qin, L., Tamasi, J., Bergenstock, M., Shapses, S., Feyen, J. H., Notterman, D. A., and Partridge, N. C. (2007) Determination of dual effects of parathyroid hormone on skeletal gene expression *in vivo* by microarray and network analysis. *J. Biol. Chem.* **282,** 33086–33097 CrossRef Medline
15. St John, H. C., Meyer, M. B., Benkusky, N. A., Carlson, A. H., Prideaux, M., Bonewald, L. F., and Pike, J. W. (2015) The parathyroid hormone-regulated transcriptome in osteocytes: parallel actions with 1,25-dihydroxyvitamin D3 to oppose gene expression changes during differentiation and to promote mature cell function. *Bone* **72,** 81–91 CrossRef Medline
16. Fu, Q., Jilka, R. L., Manolagas, S. C., and O'Brien, C. A. (2002) Parathyroid hormone stimulates receptor activator of NFκB ligand and inhibits osteoprotegerin expression via protein kinase A activation of cAMP-response element-binding protein. *J. Biol. Chem.* **277,** 48868–48875 CrossRef Medline
17. Fu, Q., Manolagas, S. C., and O'Brien, C. A. (2006) Parathyroid hormone controls receptor activator of NF-κB ligand gene expression via a distant transcriptional enhancer. *Mol. Cell. Biol.* **26,** 6453–6468 CrossRef Medline
18. Kim, S., Yamazaki, M., Shevde, N. K., and Pike, J. W. (2007) Transcriptional control of receptor activator of nuclear factor-κB ligand by the

protein kinase A activator forskolin and the transmembrane glycoprotein 130-activating cytokine, oncostatin M, is exerted through multiple distal enhancers. *Mol. Endocrinol.* **21,** 197–214 CrossRef Medline

19. Nakashima, T., Hayashi, M., Fukunaga, T., Kurata, K., Oh-Hora, M., Feng, J. Q., Bonewald, L. F., Kodama, T., Wutz, A., Wagner, E. F., Penninger, J. M., and Takayanagi, H. (2011) Evidence for osteocyte regulation of bone homeostasis through RANKL expression. *Nat. Med.* **17,** 1231–1234 CrossRef Medline
20. Xiong, J., Onal, M., Jilka, R. L., Weinstein, R. S., Manolagas, S. C., and O'Brien, C. A. (2011) Matrix-embedded cells control osteoclast formation. *Nat. Med.* **17,** 1235–1241 CrossRef Medline
21. Xiong, J., and O'Brien, C. A. (2012) Osteocyte RANKL: new insights into the control of bone remodeling. *J. Bone Miner. Res.* **27,** 499–505 CrossRef Medline
22. Saini, V., Marengi, D. A., Barry, K. J., Fulzele, K. S., Heiden, E., Liu, X., Dedic, C., Maeda, A., Lotinun, S., Baron, R., and Pajevic, P. D. (2013) Parathyroid hormone (PTH)/PTH-related peptide type 1 receptor (PPR) signaling in osteocytes regulates anabolic and catabolic skeletal responses to PTH. *J. Biol. Chem.* **288,** 20122–20134 CrossRef Medline
23. Wein, M. N., Liang, Y., Goransson, O., Sundberg, T. B., Wang, J., Williams, E. A., O'Meara, M. J., Govea, N., Beqo, B., Nishimori, S., Nagano, K., Brooks, D. J., Martins, J. S., Corbin, B., Anselmo, A., *et al.* (2016) SIKs control osteocyte responses to parathyroid hormone. *Nat. Commun.* **7,** 13176 CrossRef Medline
24. Altarejos, J. Y., and Montminy, M. (2011) CREB and the CRTC co-activators: sensors for hormonal and metabolic signals. *Nat. Rev. Mol. Cell Biol.* **12,** 141–151 CrossRef Medline
25. Hattersley, G., Dean, T., Corbin, B. A., Bahar, H., and Gardella, T. J. (2016) Binding selectivity of abaloparatide for PTH-type-1-receptor conformations and effects on downstream signaling. *Endocrinology* **157,** 141–149 CrossRef Medline
26. Kozhemyakina, E., Cohen, T., Yao, T. P., and Lassar, A. B. (2009) Parathyroid hormone-related peptide represses chondrocyte hypertrophy through a protein phosphatase 2A/histone deacetylase 4/MEF2 pathway. *Mol. Cell. Biol.* **29,** 5751–5762 CrossRef Medline
27. Dean, T., Vilardaga, J. P., Potts, J. T., Jr., and Gardella, T. J. (2008) Altered selectivity of parathyroid hormone (PTH) and PTH-related protein (PTHrP) for distinct conformations of the PTH/PTHrP receptor. *Mol. Endocrinol.* **22,** 156–166 CrossRef Medline
28. Ferrandon, S., Feinstein, T. N., Castro, M., Wang, B., Bouley, R., Potts, J. T., Gardella, T. J., and Vilardaga, J. P. (2009) Sustained cyclic AMP production by parathyroid hormone receptor endocytosis. *Nat. Chem. Biol.* **5,** 734–742 CrossRef Medline
29. Pearman, A. T., Chou, W. Y., Bergman, K. D., Pulumati, M. R., and Partridge, N. C. (1996) Parathyroid hormone induces c-fos promoter activity in osteoblastic cells through phosphorylated cAMP response element (CRE)-binding protein binding to the major CRE. *J. Biol. Chem.* **271,** 25715–25721 CrossRef Medline
30. Tyson, D. R., Swarthout, J. T., and Partridge, N. C. (1999) Increased osteoblastic c-fos expression by parathyroid hormone requires protein kinase A phosphorylation of the cyclic adenosine 3′,5′-monophosphate response element-binding protein at serine 133. *Endocrinology* **140,** 1255–1261 CrossRef Medline
31. Keller, H., and Kneissel, M. (2005) SOST is a target gene for PTH in bone. *Bone* **37,** 148–158 CrossRef Medline
32. Shimizu, E., Selvamurugan, N., Westendorf, J. J., Olson, E. N., and Partridge, N. C. (2010) HDAC4 represses matrix metalloproteinase-13 transcription in osteoblastic cells, and parathyroid hormone controls this repression. *J. Biol. Chem.* **285,** 9616–9626 CrossRef Medline
33. Shimizu, E., Nakatani, T., He, Z., and Partridge, N. C. (2014) Parathyroid hormone regulates histone deacetylase (HDAC) 4 through protein kinase A-mediated phosphorylation and dephosphorylation in osteoblastic cells. *J. Biol. Chem.* **289,** 21340–21350 CrossRef Medline
34. Wein, M. N., Spatz, J., Nishimori, S., Doench, J., Root, D., Babij, P., Nagano, K., Baron, R., Brooks, D., Bouxsein, M., Pajevic, P. D., and Kronenberg, H. M. (2015) HDAC5 controls MEF2C-driven sclerostin expression in osteocytes. *J. Bone Miner. Res.* **30,** 400–411 CrossRef Medline
35. Huang, J. C., Sakata, T., Pfleger, L. L., Bencsik, M., Halloran, B. P., Bikle, D. D., and Nissenson, R. A. (2004) PTH differentially regulates expression of RANKL and OPG. *J. Bone Miner. Res.* **19,** 235–244 Medline
36. Galli, C., Fu, Q., Wang, W., Olsen, B. R., Manolagas, S. C., Jilka, R. L., and O'Brien, C. A. (2009) Commitment to the osteoblast lineage is not required for RANKL gene expression. *J. Biol. Chem.* **284,** 12654–12662 CrossRef Medline
37. Tseng, W., Graham, L. S., Geng, Y., Reddy, A., Lu, J., Effros, R. B., Demer, L., and Tintut, Y. (2010) PKA-induced receptor activator of NF-κB ligand (RANKL) expression in vascular cells mediates osteoclastogenesis but not matrix calcification. *J. Biol. Chem.* **285,** 29925–29931 CrossRef Medline
38. Yang, D. C., Tsay, H. J., Lin, S. Y., Chiou, S. H., Li, M. J., Chang, T. J., and Hung, S. C. (2008) cAMP/PKA regulates osteogenesis, adipogenesis and ratio of RANKL/OPG mRNA expression in mesenchymal stem cells by suppressing leptin. *PLoS ONE* **3,** e1540 CrossRef Medline
39. Aggen, J. B., Nairn, A. C., and Chamberlin, R. (2000) Regulation of protein phosphatase-1. *Chem. Biol.* **7,** R13–R23 CrossRef Medline
40. MacKintosh, C., Campbell, D. G., Hiraga, A., and Cohen, P. (1988) Phosphorylation of the glycogen-binding subunit of protein phosphatase-1G in response to adrenalin. *FEBS Lett.* **234,** 189–194 CrossRef Medline
41. Okamura, H., Yang, D., Yoshida, K., and Haneji, T. (2013) Protein phosphatase 2A Cα is involved in osteoclastogenesis by regulating RANKL and OPG expression in osteoblasts. *FEBS Lett.* **587,** 48–53 CrossRef Medline
42. Janssens, V., and Goris, J. (2001) Protein phosphatase 2A: a highly regulated family of serine/threonine phosphatases implicated in cell growth and signalling. *Biochem. J.* **353,** 417–439 Medline
43. Obri, A., Makinistoglu, M. P., Zhang, H., and Karsenty, G. (2014) HDAC4 integrates PTH and sympathetic signaling in osteoblasts. *J. Cell Biol.* **205,** 771–780 CrossRef Medline
44. Henriksson, E., Jones, H. A., Patel, K., Peggie, M., Morrice, N., Sakamoto, K., and Göransson, O. (2012) The AMPK-related kinase SIK2 is regulated by cAMP via phosphorylation at Ser358 in adipocytes. *Biochem. J.* **444,** 503–514 CrossRef Medline
45. Dean, T., Linglart, A., Mahon, M. J., Bastepe, M., Jüppner, H., Potts, J. T., Jr., and Gardella, T. J. (2006) Mechanisms of ligand binding to the parathyroid hormone (PTH)/PTH-related protein receptor: selectivity of a modified PTH(1–15) radioligand for GαS-coupled receptor conformations. *Mol. Endocrinol.* **20,** 931–943 CrossRef Medline
46. Okamura, H., Yoshida, K., Ochiai, K., and Haneji, T. (2011) Reduction of protein phosphatase 2A Cα enhances bone formation and osteoblast differentiation through the expression of bone-specific transcription factor Osterix. *Bone* **49,** 368–375 CrossRef Medline
47. Henriksson, E., Säll, J., Gormand, A., Wasserstrom, S., Morrice, N. A., Fritzen, A. M., Foretz, M., Campbell, D. G., Sakamoto, K., Ekelund, M., Degerman, E., Stenkula, K. G., and Göransson, O. (2015) SIK2 regulates CRTCs, HDAC4 and glucose uptake in adipocytes. *J. Cell Sci.* **128,** 472–486 CrossRef Medline
48. Itoh, Y., Sanosaka, M., Fuchino, H., Yahara, Y., Kumagai, A., Takemoto, D., Kagawa, M., Doi, J., Ohta, M., Tsumaki, N., Kawahara, N., and Takemori, H. (2015) Salt-inducible kinase 3 signaling is important for the gluconeogenic programs in mouse hepatocytes. *J. Biol. Chem.* **290,** 17879–17893 CrossRef Medline
49. Lombardi, M. S., Gilliéron, C., Berkelaar, M., and Gabay, C. (2017) Salt-inducible kinases (SIK) inhibition reduces RANKL-induced osteoclastogenesis. *PLoS ONE* **12,** e0185426 CrossRef Medline
50. Patel, K., Foretz, M., Marion, A., Campbell, D. G., Gourlay, R., Boudaba, N., Tournier, E., Titchenell, P., Peggie, M., Deak, M., Wan, M., Kaestner, K. H., Göransson, O., Viollet, B., Gray, N. S., Birnbaum, M. J., Sutherland, C., and Sakamoto, K. (2014) The LKB1-salt-inducible kinase pathway functions as a key gluconeogenic suppressor in the liver. *Nat. Commun.* **5,** 4535 CrossRef Medline
51. Weir, E. C., Philbrick, W. M., Amling, M., Neff, L. A., Baron, R., and Broadus, A. E. (1996) Targeted overexpression of parathyroid hormone-related peptide in chondrocytes causes chondrodysplasia and delayed endochondral bone formation. *Proc. Natl. Acad. Sci. U.S.A.* **93,** 10240–10245 CrossRef Medline
52. Sasagawa, S., Takemori, H., Uebi, T., Ikegami, D., Hiramatsu, K., Ikegawa, S., Yoshikawa, H., and Tsumaki, N. (2012) SIK3 is essential for chondro-

cyte hypertrophy during skeletal development in mice. *Development* **139,** 1153–1163 CrossRef Medline

53. Kim, J. H., Hedrick, S., Tsai, W. W., Wiater, E., Le Lay, J., Kaestner, K. H., Leblanc, M., Loar, A., and Montminy, M. (2017) CREB coactivators CRTC2 and CRTC3 modulate bone marrow hematopoiesis. *Proc. Natl. Acad. Sci. U.S.A.* **114,** 11739–11744 CrossRef Medline
54. Martowicz, M. L., Meyer, M. B., and Pike, J. W. (2011) The mouse RANKL gene locus is defined by a broad pattern of histone H4 acetylation and regulated through distinct distal enhancers. *J. Cell. Biochem.* **112,** 2030–2045 CrossRef Medline
55. Onal, M., St John, H. C., Danielson, A. L., and Pike, J. W. (2016) Deletion of the distal Tnfsf11 RL-D2 enhancer that contributes to PTH-mediated RANKL expression in osteoblast lineage cells results in a high bone mass phenotype in mice. *J. Bone Miner. Res.* **31,** 416–429 CrossRef Medline
56. Usui, H., Inoue, R., Tanabe, O., Nishito, Y., Shimizu, M., Hayashi, H., Kagamiyama, H., and Takeda, M. (1998) Activation of protein phosphatase 2A by cAMP-dependent protein kinase-catalyzed phosphorylation of the 74-kDa B″ (delta) regulatory subunit *in vitro* and identification of the phosphorylation sites. *FEBS Lett.* **430,** 312–316 CrossRef Medline
57. Ahn, J. H., McAvoy, T., Rakhilin, S. V., Nishi, A., Greengard, P., and Nairn, A. C. (2007) Protein kinase A activates protein phosphatase 2A by phosphorylation of the B56δ subunit. *Proc. Natl. Acad. Sci. U.S.A.* **104,** 2979–2984 CrossRef Medline
58. Feschenko, M. S., Stevenson, E., Nairn, A. C., and Sweadner, K. J. (2002) A novel cAMP-stimulated pathway in protein phosphatase 2A activation. *J. Pharmacol. Exp. Ther.* **302,** 111–118 CrossRef Medline
59. Screaton, R. A., Conkright, M. D., Katoh, Y., Best, J. L., Canettieri, G., Jeffries, S., Guzman, E., Niessen, S., Yates, J. R., 3rd, Takemori, H., Okamoto, M., and Montminy, M. (2004) The CREB coactivator TORC2 functions as a calcium- and cAMP-sensitive coincidence detector. *Cell* **119,** 61–74 CrossRef Medline
60. Lee, C. W., Yang, F. C., Chang, H. Y., Chou, H., Tan, B. C., and Lee, S. C. (2014) Interaction between salt-inducible kinase 2 and protein phosphatase 2A regulates the activity of calcium/calmodulin-dependent protein kinase I and protein phosphatase methylesterase-1. *J. Biol. Chem.* **289,** 21108–21119 CrossRef Medline